Applied Catalysis B: Environmental 215 (2017) 85–92

Contents lists available at ScienceDirect

Applied Catalysis B: Environmental

journal homepage: www.elsevier.com/locate/apcatb

Controlling charge transfer in quantum-size titania for photocatalytic applications

Songling Wang[a,b,1], Shuhai Lin[d,1], Dieqing Zhang[c,*], Guisheng Li[c], Michael K.H. Leung[b,*]

[a] Department of Chemistry, National University of Singapore, 117543, Singapore
[b] Ability R&D Energy Research Centre, School of Energy and Environment, City University of Hong Kong, Hong Kong, China
[c] Key Laboratory of Resource Chemistry of Ministry of Education, Shanghai Key Laboratory of Rare Earth Functional Materials, Shanghai Normal University, Shanghai 200234, China
[d] Department of Biochemistry and Molecular Cell Biology, Shanghai Key Laboratory for Tumor Microenvironment and Inflammation, Shanghai Jiao Tong University School of Medicine, Shanghai 200025, China

ARTICLE INFO

Article history:
Received 1 March 2017
Received in revised form 12 May 2017
Accepted 15 May 2017
Available online 17 May 2017

Keywords:
Photocatalysis
Charge transfer
Solar light harvesting
Quantum-size TiO_2
Environmental remediation

ABSTRACT

Separation and migration of the charge carriers to the surface of semiconductor catalysts are of fundamental importance for efficient photocatalytic reactions. The interior recombination of charge carriers is detrimental to photocatalytic efficiency of catalysts. Reduction in particle size of catalysts in principle promotes charge transport to surface by shortening the migration path. The quantum size is promising for dissociating excitons into free electrons and holes in three spatial dimensions. Herein, we report the quantum-size titania (Q-TiO_2) particles (2–3 nm) synthesized via a microwave-assisted rout. Combining quantum size and molecular-semiconductor interfacial effect enables more reactive sites exposure and greatly promotes charge transport from interior to surface of Q-TiO_2. Hence, the Q-TiO_2 catalyst gave rise to significantly improved photocatalytic performances with visible light ($\lambda \geq 420$ nm): bacteria (*E. coli*) disinfection and organic pollutant (RhB) degradation. Taken together, this finding highlights the key importance of specific surface states to take into account high charge-carrier transfer and separation for photocatalytic environmental remediation.

1. Introduction

The sustainable development of photocatalysis is to transform chemicals efficiently with solar energy in environmental and clean energy fields [1–3]. The recombination of excited electrons and holes, so far, is a critical problem and limits the efficiencies of photocatalytic activities [4]. A long-time survival and mobility of the excitons must be sufficient to allow them to migrate to the surface of catalysts for photocatalytic redox reactions. Noticeably, for semiconductors, the excited electrons and holes relax to the conduction band minimum (CB) and valence band maximum (VB), respectively [5]. This relaxation process is related to the carrier cooling dynamics [6]. The pristine bulk semiconductors give a fast relaxation as a result of connective valence and conductive bands. While the excitons for the quantum-size particles relax at a much slower rate due to the discreteness in the energy levels and hence undergo longer cooling time [6]. From the theory standpoint, the discreteness in valence and conduction energy bands, consequently, gives rise to an increase in the lifetimes of the excited electrons and holes. On the other hand, small size should promote charge transport to the catalyst surface because of the dramatically increased surface-to-volume ratio, hence accelerating the photocatalytic redox reactions [7,8].

Titania as catalyst has been extensively studied for photocatalytic waste purification and water splitting owing to its suitable band edge, stability, and low cost [1,9–13]. However, the rapid recombination of photo-induced electron-hole carriers in drawback TiO_2 material limits its efficient photocatalytic activities [14,15]. Fortunately, light-induced electrons transfer can be controlled at molecular-semiconductor interfaces based on the reported literature [15,16]. Exploring quantum-size TiO_2 catalyst, thereby, is a promissing strategy allowing for the migration of charge carriers from interior to the surface, reducing charge-carrier recombination within TiO_2 particles. Although the band gap of quantum-size TiO_2 suffers broadened due to quantum confinement effect [17–19], engineering its surface states, e.g., Ti^{3+}-oxygen

* Corresponding authors.
E-mail addresses: dqzhang@shnu.edu.cn (D. Zhang), mkh.leung@cityu.edu.hk (M.K.H. Leung).
[1] The contribution of Wang and Lin is equal.

http://dx.doi.org/10.1016/j.apcatb.2017.05.043
0926-3373/

vacancies [15,20], can potentially narrow its band gap to response visible light.

To combine the advantages of quantum-size and specific surface states, we synthesized the quantum-size TiO_2 particles (2–3 nm) *via* a microwave-assisted reaction. The quantum size strengthens charge carriers separation by shortening the migration path to the particle surface. On the other hand, the presence of surface Ti^{3+}- oxygen vacancies ($OV_{surface}$) association promotes the valence band position and hence reduces the band gap of quantum-size TiO_2 shell. Additionally, the holes' trapping by surface organic capping groups competes with charge carrier recombination occurring within the quantum-size iO_2 particles, releasing excited electrons. These priorities have profound implications in producing a long-time survival of photo-induced charge carriers that are essential for photocatalytic activities. Herein, our results indicate that Q-TiO_2 catalyst gave rise to significantly improved photocatalytic performances with visible light ($\lambda \geq 420$ nm): bacteria (*E. coli*) disinfection and organic pollutant (RhB) degradation.

2. Experimental section

2.1. Chemicals and characterizations

Titanium tetrachloride and ethylene glycol were purchased from Sigma-Aldrich. Transmission electron microscopy (TEM), high-resolution TEM (HR-TEM) were performed on TEI Tecnai G220 Scaning TEM. X-Ray Diffraction (XRD) patterns were recorded on D/MAX-2000 diffractometer with high-intensity CuKα irradiation ($\lambda = 1.5406$ Å). X-Ray photoelectron spectroscopy (XPS) measurements were done on Perkin-Elmer PHI 5000C XPS system with a monochromatic Al-Kα source and a charge neutralizer. UV–vis absorption and diffuse reflectance spectra (DRS) were measured using a Shimadzu UV-2600 spectrophotometer. Gas chromatography-mass spectrometry (GC–MS) was tested on the Agilent GC/MS (Agilent 7890A GC/Agilent 5975C MS). The photoluminescence (PL) emission spectra were collected on FluoroMax-4 spectrofluorometer with the excitation wavelength 325 nm. Lifetime measurement was performed on the Fluorolog spectrofluorometer. X-ray absorption spectroscopy (XAS) data was recorded on the testing system in Singapore synchrotron radiation center.

2.2. Synthesis of the quantum-size TiO_2 (Q-TiO_2) particles

Titanium tetrachloride ($TiCl_4$) of 0.05 mL was dropped into 10 mL ethylene glycol at room temperature. After stirring for around 30 min, the above solution was transferred into a 50 mL Teflon cell for microwave reactions at 160 °C and power 800 W, for 10 min. After reactions, the microwave system stopped and the Teflon cell with product solution cooled down to room temperature. Then, the clear and transparent product solution was washed with ethanol and deionized water 3–4 times. Finally, the precipitant (Q-TiO_2) obtained was maintained in ethylene glycol.

2.3. Synthesis of the TiO_2 sheets

The TiO_2 sheets sample was prepared by removing organic ligands capping groups of Q-TiO_2 particles. Under stirring, acetone was used to dissolve the organic capping groups of Q-TiO_2 material at 30 °C. The white *TiO_2 sheets* powder was obtained after freeze drying in vacuum chamber.

2.4. Contact angle measurement

The mixed solution containing 10 mg of the as-prepared Q-TiO_2 and 3.0 mL of ethanol undergone ultrasonication for 5 min followed by depositing to the glass substrate to form a thin film. This glass substrate was kept in oven with 30 °C, and finally the dried thin film was obtained. The P25 thin film was also fabricated with the same procedure. Both of the dried thin film samples were ready for contact angle measurement.

2.5. Degradation of rhodamine B (RhB)

50 mg of Q-TiO_2 sample was added into Rhodamine B aqueous solution (50 mL, 10 mg/L) followed by ultrasonication for 10 min. Under magnetic stirring at room temperature, such solution was kept in dark for saturated adsorption of RhB. 5 mL of the solution was sampled at 20, 40, 60, and 80 min, respectively, and centrifuged to remove the precipitate Q-TiO_2 material and get the supernatant solution. After saturated adsorption, the degradation of RhB was carried out under visible light irradiation ($\lambda \geq 420$ nm). A 500-W Xe lamp fixed with a light filter was used as light source with the wavelength $\lambda \geq 420$ nm. The concentration of RhB remained in solution was tested by UV–vis absorption spectrophotometer. For comparison, the degradation of RhB over pristine TiO_2 (P25) was also tested under the same procedure.

2.6. Disinfection of bacteria (E. coli)

The *E. coli* (Invitrogen Life Technologies) culture was incubated in a LB broth (Tissue culture grade, Amresco) at 35 °C for 12 h. Then the *E. coli* suspension was obtained after centrifugation the above culture at 4000 rpm for 2 min. To ensure sterilization, Q-TiO_2 was mixed with 0.9 wt.% NaCl (Sigma-Aldrich) solution in a media bottle (200 mL) followed by ultrasonication for 5 min and autoclave at 120 °C for 40 min. The Q-TiO_2 of 0.2 mg/mL was detected for the disinfection effect on water contaminated with *E. coli*. All the tests were performed at room temperature under magnetic stirring. The light source is a 300-W Xe lamp (100 mW/cm^2) with a light filter 5 μL of the reaction suspension was sampled every 5 min interval and immediately transferred into the biosafety cabinet for spreading on the nutrient Agar and LB broth plate of petri dish. After incubation at 37 °C for 24 h, the colony forming units of *E. coli* were counted to determine the survival ratio. Besides, the disinfection over TiO_2 sheets and P25 nanoparticles was conducted under the same procedure for comparison.

3. Results and discussion

The synthesis of quantum-size TiO_2 particles was inspired by our reported method for fabrication of WO_3 quantum dots [21]. We used ethylene glycol as reactant and solvent to control the quantum size via reducing the hydrolysis rate of Ti^{4+} with water molecules produced by the condensation reaction of ethylene glycol molecules. The condensation reaction was also identified by the by-products chain-like ethers found in the as-prepared TiO_2 solution, as shown by the GC–MS (Fig. S1). We also studied the synthesis process of the quantum-size TiO_2 particles. The TEM image (Fig. S2a) shows that the organic-titania composite was first formed after reaction time for 2 min. Then such composite decomposed and released titania particles after 5-min reaction (Fig. S2b). Finally, the ultrafine TiO_2 particles (Fig. S2c) were achieved after reaction for 10 min.

The XRD technique was used to investigate the phase structure of the synthesized TiO_2 particles. As shown in Fig. 1a, three main diffraction peaks (101), (004), and (200) were indexed to the anatase phase TiO_2 (JCPDS No. 21-1272). The TEM images (Fig. 1b and c) display the homogeneous and ultrafine nanoparticles. The HR-TEM image further presents their crystalline structures in Fig. 1d. The crystal lattices 0.35 and 0.38 nm are corresponding

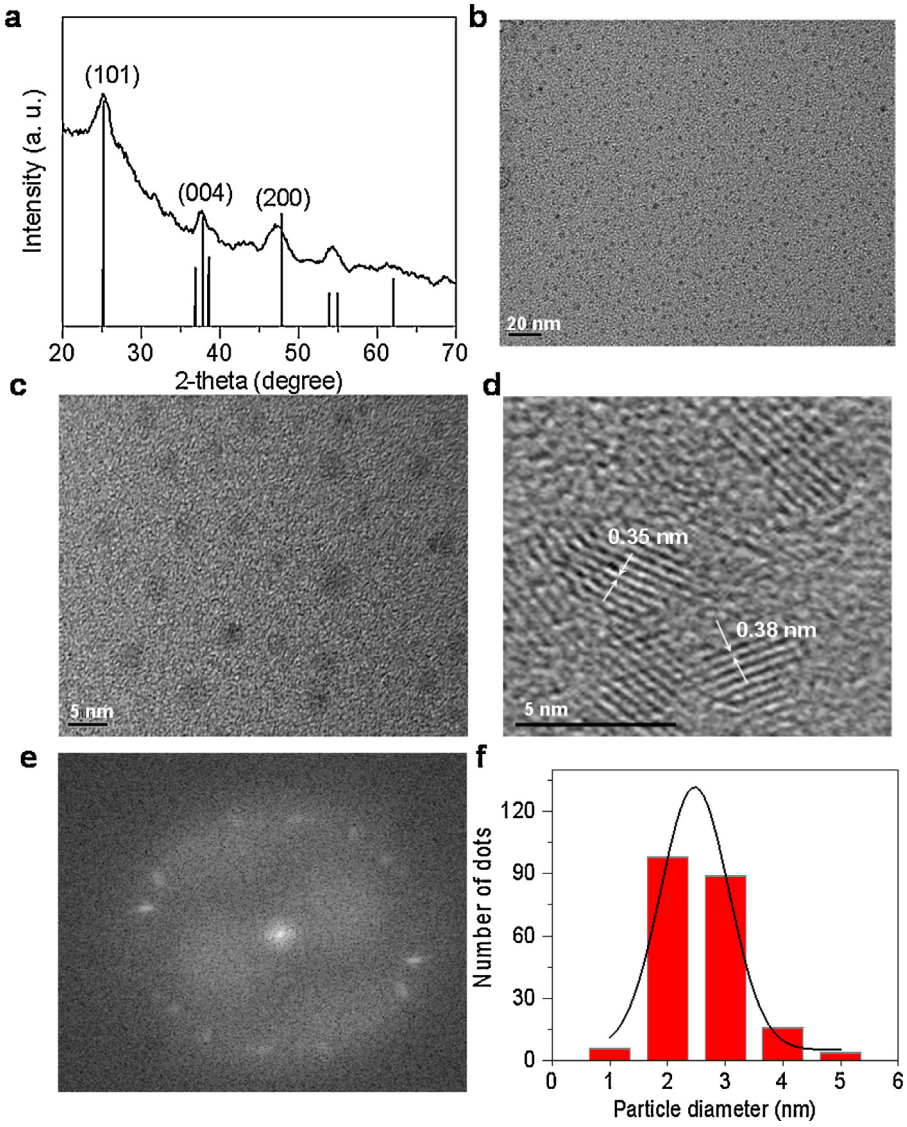

Fig. 1. Structure and morphology characterizations of the as-prepared Q-TiO_2: (a) XRD patterns, (b) and (c) TEM images, (d) HR-TEM image, (e) FFT image, (f) Size distribution obtained based on TEM image (a).

to the (101) and (200) facets of anatase TiO_2, respectively. Furthermore, the fast fourier transformation (FFT) image (Fig. 1e) displays multi-crystal patterns because of the ultrafine particles. The size in diameter was statistically counted based on the TEM image (Fig. 1b). A narrow size distribution is centered at around 2–3 nm in Fig. 1f.

The chemical states and compositions of the quantum-size TiO_2 (Q-TiO_2) particles were investigated by using XPS. The XPS C 1 s peak with a binding energy at 284.6 eV was used as a reference to calibrate XPS peaks [22]. The survey XPS spectra (Fig. S3a) displays that the Q-TiO_2 sample gave the clear signals of O 1s, Ti 2p, C 1s, Cl 2p, and Ti 3p species. The carbon element is presumably from organic ligands and the adventitious hydrocarbon from XPS instrument itself. The core level Ti $2p_{3/2}$ peak (Fig. 2a) with the binding energy at 458.8 eV is indicative of the Ti^{4+} (TiO_2) [23,24]. However, the Ti 2p XPS peaks of Q-TiO_2 are broader in comparison with that of P25. In particular, a shoulder intensity circled with blue line appears at the lower binding energy side (Fig. 2a). The overall feature of Ti $2P_{3/2}$ peak (Fig. 2b) can be deconvoluted into two main peaks: Ti^{4+} (458.8 eV) and Ti^{3+} (457.7 eV) [25]. The presence of Ti^{3+} suggests the formation of oxygen vacancies ($OV_{surface}$) on the surface of Q-TiO_2 catalyst. Note that creating $OV_{surface}$ in TiO_2 catalyst not only improves visible light absorption but also provides active sites and increases the electron donor density to promote charge transport, thus enhancing the photocatalytic activities with low-energy photons, such as degradation of organic pollutants for water purification [25–27]. Furthermore, the core level Cl $2p_{3/2}$ XPS peak (Fig. S3b) was found at 198.0 eV, which is attributed to the adsorbed Cl^- from $TiCl_4$ reactant [28]. It should be noted that the lattice O in O–Ti–O structure cannot be substituted by Cl element as the atomic radius of Cl (1.81 Å) is larger than that of O (1.40 Å) [29,30]. Furthermore, in Fig. 1a, we also did not find peak shift originated from lattice-dopant species. In other words, Cl element is surface-doped, not lattice-doped, and thus reducing recombination sites relating to lattice-dopant species. Here, it is deduced that the Cl^- species probably replaced the surface OH groups of Q-TiO_2, that is, some surface O–Ti–OH groups were substituted by O–Ti–Cl. Another possible reason is Cl^- species chemically bonded to surface unsaturated titanium species of Q-TiO_2 particles: O–Ti– → O–Ti–Cl. Both of these reasons created $OV_{surface}$ on the surface of Q-TiO_2 particles and hence formed $OV_{surface}$ shell. To confirm this, we also conducted the electron spin resonance (ESR) spectroscopy

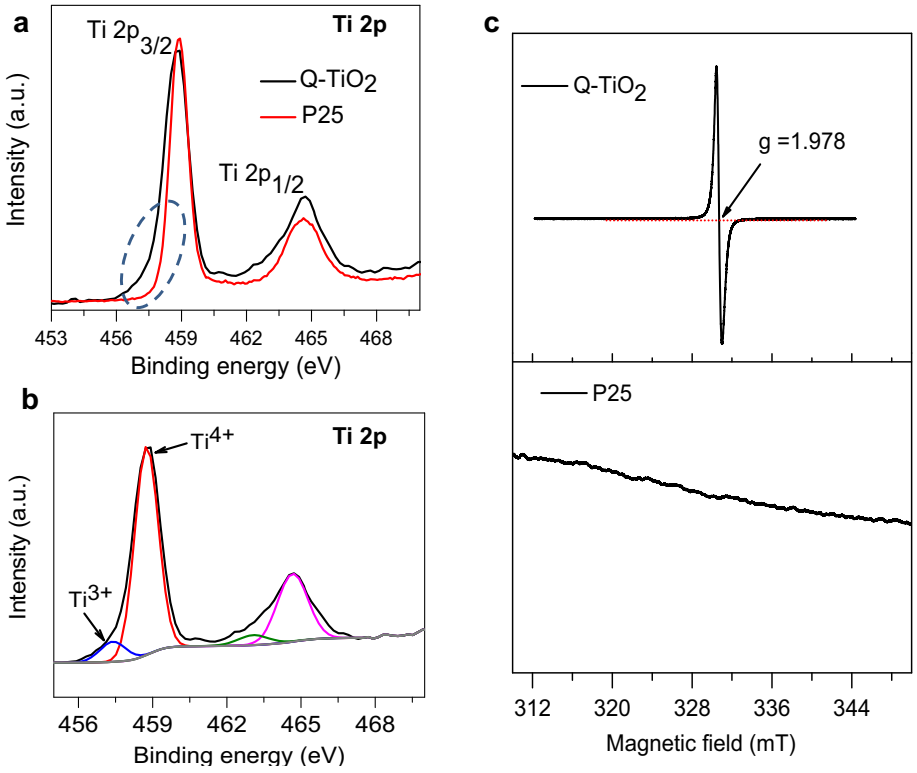

Fig. 2. (a) Core level XPS Ti 2p spectra of the Q-TiO_2 and P25, (b) XPS Ti 2p fitting spectra of the Q-TiO_2, (c) ESR spectra of the Q-TiO_2 and P25.

to identify the existence of surface Ti^{3+} stemming from the $OV_{surface}$ [25,27]. Noticeably, the surface Ti^{3+} generally, gives rise to a broad signal shape in comparison with that of interior [25,31]. As indicated in Fig. 2c, the Q-TiO_2 sample presents a g value of 1.978, which responds to the surface Ti^{3+}-oxygen vacancy association [20,25,32], whereas such signal was not found for P25.

To further investigate the specific surface states, FTIR measurement was conducted to indicate the organic ligands capping groups. In in comparison with P25, several new absorption peaks were observed over Q-TiO_2 in Fig. S4. A new band 1082 cm^{-1} was attributable to the coupled stretching υ(C—O), υ(C—C) and deformation δ (CH_2) modes [33]. The band at 1360 cm^{-1} was the diagnostic of the formation of HO—CH_2—COO^- [34]. The two peaks positioned at 2874 and 2952 cm^{-1} were ascribed to the —C—H vibrations [35]. Based on literature, organic capping groups play a particular role in controlling the surface states of catalysts, such as narrowing band gap and increasing charge transfer of TiO_2 through modifying pristine phase with organic ligands [7,21,36]. Furthermore, such capping agents could create specific surface states including hydrophobicity, charge density, and zeta potentials, etc. [37]. For instance, the surface hydrophobicity of Q-TiO_2 material was increased as a result of the presence of organic capping groups. We also studied the surface hydrophobicity via testing water contact angle. As shown in Fig. 3a, the contact angle was far from 0° even when one water drop stayed on the surface of Q-TiO_2 for 90 s. By contrast, the contact angle for P25 sample almost became to 0° after only 5 s in Fig. 3b. We concluded that the organic ligands capping groups enabled Q-TiO_2 more hydrophobicity and less wettability than P25. Particularly, the critical point of the capping groups is related to the charge-carrier separation. With regard to the colloidal TiO_2, the recombination of electrons with free holes is about 10 times faster than holes trapping, according to the reported literature [38]. This interprets why the ultrafine TiO_2 catalyst is required to fast move free holes to its surface, which is particularly important to avoid recombination occurring within particles [38,39]. The excited holes in trapped state are relatively unreactive toward the excited electrons which can survive for many microseconds [38,40]. As previous literature reported, the trapping of photo-induced holes by surface organic groups competes with the charge carriers recombination [40]. Here we further provided experimental evidences with respect to the higher separation and longer survival time of charge carrier. After removing capping groups of Q-TiO_2, the particles could connect together and become sheet structure, as displayed in scheme (Fig. S5a). Indeed, TEM and HR-TEM images clearly exhibit sheet morphology and lattice structure (Fig. S5b). Furthermore, the important point regarding separation and survival time of photo-induced charge carriers were studied by photoluminescence (PL) emission and lifetime measurements. As indicated in Fig. 4a, the Q-TiO_2 particles presented lower PL emission intensity compared to the TiO_2 sheets, implying higher charge carrier separation rates [28]. On the other hand, the Q-TiO_2 particles gave rise to a longer survival time of photo-induced charge carriers, which was verified by lifetime test in Fig. 4b. This is consistent with the phenomenon that organic molecules could potentially improve charge transfer and separation [16].

Noticeably, the shift of valence band for TiO_2 material is much larger than that of conduction band as the holes with much less mass than electrons can relax at a fast rate [6]. Hence, the holes can undergo larger size-quantization effects [6]. For this reason, the transfer of the created free holes from VB1 to VB2 is faster than recombination with electrons within particles, leading to holes trapping by the capping groups (Scheme 1b) [41]. In this case, the photo-induced charge carriers can be effectively separated, thus releasing massive excited electrons and holes. To further interpret this phenomenon, the ESR studies were carried out to test the active oxygen species ($^{\bullet}O_2^-$ and $^{\bullet}OH$) [37]. Here, we used the 5, 5-dimethyl-1-pyrroline-N-oxide (DMPO) as spin-trap reagent. The DMPO-$^{\bullet}O_2^-$ and DMPO-$^{\bullet}OH$ radicals can arise from the reactions of electrons with O_2 and holes with hydroxyl group or water molecule, respectively [20,42,43]. In comparison with TiO_2 sheets, the Q-TiO_2

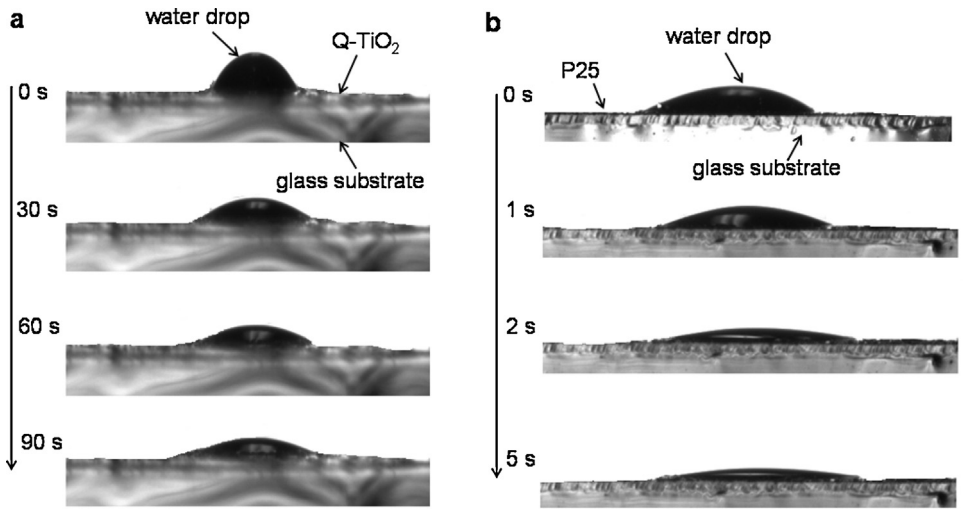

Fig. 3. Surface wettability characterizations by using time-dependent water contact angle tests: (a) Photographs of Q-TiO_2 taken from 0 to 90 s, (b) Photographs of P25 taken from 0 to 5 s.

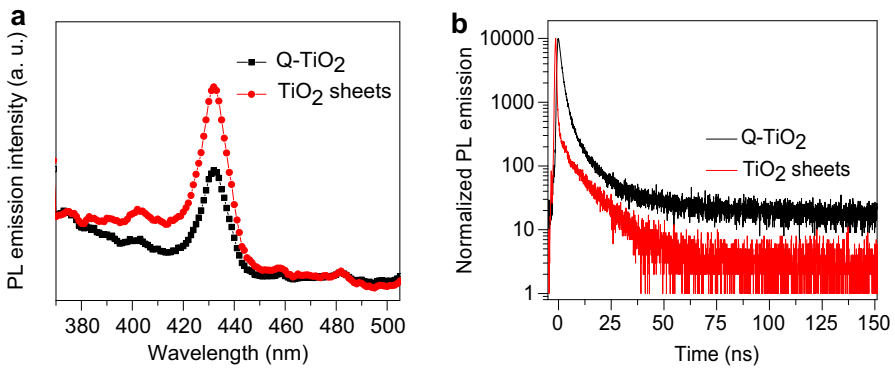

Fig. 4. Characterizations of charge-carrier separation in Q-TiO_2 and TiO_2 sheets: photoluminescence emission (PL) spectra excited with 325 nm (a) and time-dependent lifetime of excited charge carriers with the excitation of 374 nm laser and emission wavelength at 431 nm.

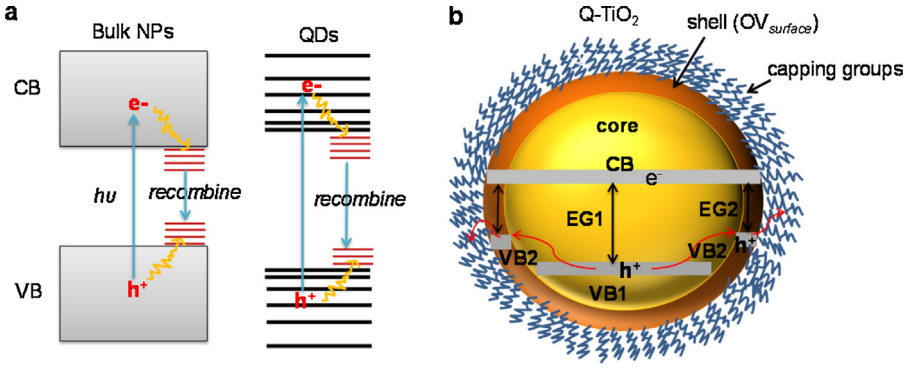

Scheme 1. (a) Schematic diagrams of the photo-induced electrons and holes transfer of the bulk nanoparticles (NPs) and quantum dots (QDs) under light irradiation; (b) Schematic charge transfer at shell and core of the Q-TiO_2 under light irradiation.

sample exhibited stronger O_2^- and •OH signals after optical excitation ($\lambda \geq 420$ nm), as shown in Fig. 5a and b. However, both $^{\bullet}O_2^-$ and •OH actives for P25 nanoparticles were not detectable. This ESR result suggests that more excited electrons and holes transferred from the interior to the surface of Q-TiO_2, which are expected for photocatalytic properties.

Apart from the surface study of Q-TiO_2 material, we also investigated its band structure including valance band maximum (VBM) and conduction band (CBM) positions as well as bandgap energy by using UPS, XAS, and UV–vis DRS techniques. Normally, Fermi level is set at 0.0 eV. Fig. 6a shows VBM positions of Q-TiO_2 and commercial TiO_2 (P25) samples. The VBM-1 for Q-TiO_2 and VBM-2 for P25 are around 1.81 eV and 2.05 eV, respectively. This suggests that the VBM-1 has been promoted around 0.24 eV compared with that of P25. It is presumably associated with the $OV_{surface}$ sites [30]. However, the XAS result (Fig. 6b) shows that there were no apparent differences of CBM positions (t_{2g}) over the Q-TiO_2 material and P25. Although the two materials presented a same CBM position,

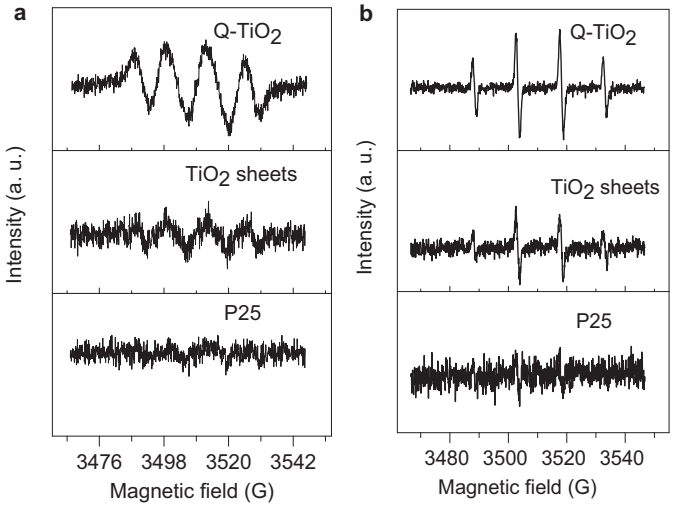

Fig. 5. ESR spectra of the Q-TiO_2, TiO_2 sheets, and P25 materials under visible light irradiation ($\lambda \geq 420$ nm): (a) DMPO-$^{\bullet}O_2^-$ adducts characterized in benzyl alcohol, (b) DMPO-$^{\bullet}$OH adducts tested in water. The commercial P25 was used for comparison.

Q-TiO_2 had relatively reduced intensity of t_{2g} peak, which was originated from the presence of Ti^{3+} associated with $OV_{surface}$. This XAS result together with the UPS analysis suggests that the $OV_{surface}$ caused by Ti^{3+} and organic ligands capping groups promote the VB level towards Fermi level, rather than changing the CBM position. For the bandgap energy, the Q-TiO_2 sample gives rise to a red-shift and higher absorption intensity in the visible light region in comparison with P25 in Fig. 6c. Based on Kubelka-Munk functions, the bandgap absorption edge of Q-TiO_2 sample is 2.83, smaller than 3.05 eV of P25, as indicated by the UV–vis DRS spectra (Fig. 6d). Taken together, the presence of $OV_{surface}$ promoted the valence band position and consequently reduced the bandgap of Q-TiO_2 shell [33,44,45]. As shown in Scheme 1b, the valence band (VB2) at surface is higher than VB1 at core, leading to a narrower bandgap energy (BG2) at shell than BG1 at core of Q-TiO_2 particles. Thereby, the UPS, XAS, and UV–vis DRS results strongly support Scheme 1.

We examined photocatalytic performances of Q-TiO_2 particles on water purification and disinfection of bacterial with visible light ($\lambda \geq 420$ nm). For water purification, we used the organic dye rhodamine B (RhB) as a probe to evaluate the photocatalytic property of Q-TiO_2 catalyst. The concentration of RhB aqueous solution was determined by UV–vis absorption spectrum. The TiO_2 sheets and P25 materials were used for comparison. After saturated adsorption in dark (light off, around 40 min), RhB molecules were removed by 89% for Q-TiO_2, 58% for TiO_2 sheets, and 18% for P25 under light irradiation for 60 min (see Figs. 7 a, b, and S6). In addition to water purification, we also detected the disinfection of bacterial *Escherichia coli* (*E. coli*) with visible light ($\lambda \geq 420$ nm). As shown in Fig. 7c, the bacteria *E. coli* over the Q-TiO_2 catatlys were almost disinfected in 25 min. The corresponding pictures of the *E. coli* cultured in petri-dishes (Fig. 7d) have been taken with different illumination time. While the survival rates of P25 and TiO_2 sheets catalysts were even up to around 85% and 20%, respectively, indicating that a great number of the *E. coli* still survived. The control experiments (no light and no catalyst) exhibited no obvious changes of E. coli survival rates. Therefore, the shortening charge transfer path from interior to the surface of small particles improves the photo-induced electron-hole separation, enhancing photocatalytic performances.

4. Conclusions

The quantum-size TiO_2 (Q-TiO_2) particles were successfully synthesized *via* a microwave-assisted approach. The combination of small size and specific surface states gives rise to new properties: (1) short migration path of charge carriers; (2) promoted valence band position and narrowed bandgap of shell; (3) higher charge-carrier separation. These priorities have profound implications in controlling charge transfer from interior to the surface of catalyst for solar light harvesting. The synthesized Q-TiO_2 catalyst exhibited great improvement in photocatalytic performances with visible light ($\lambda \geq 420$ nm): bacteria (*E. coli*) disinfection and organic pollu-

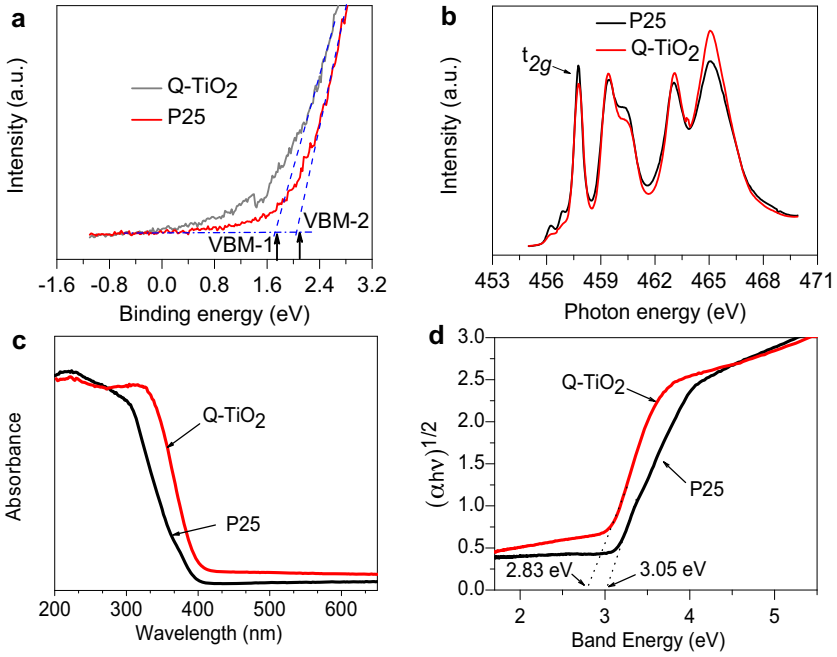

Fig. 6. Band structure characterizations of Q-TiO_2 and P25 mateirals: valance band and conduction band positions measured by (a) UPS and (b) XAS; Bandgap energy identified by (c) UV–vis absorption spectra and (d) UV–vis DRS spectra obtaind based on Kubelka-Munk function transformation for the calculated absorption versus photon energy.

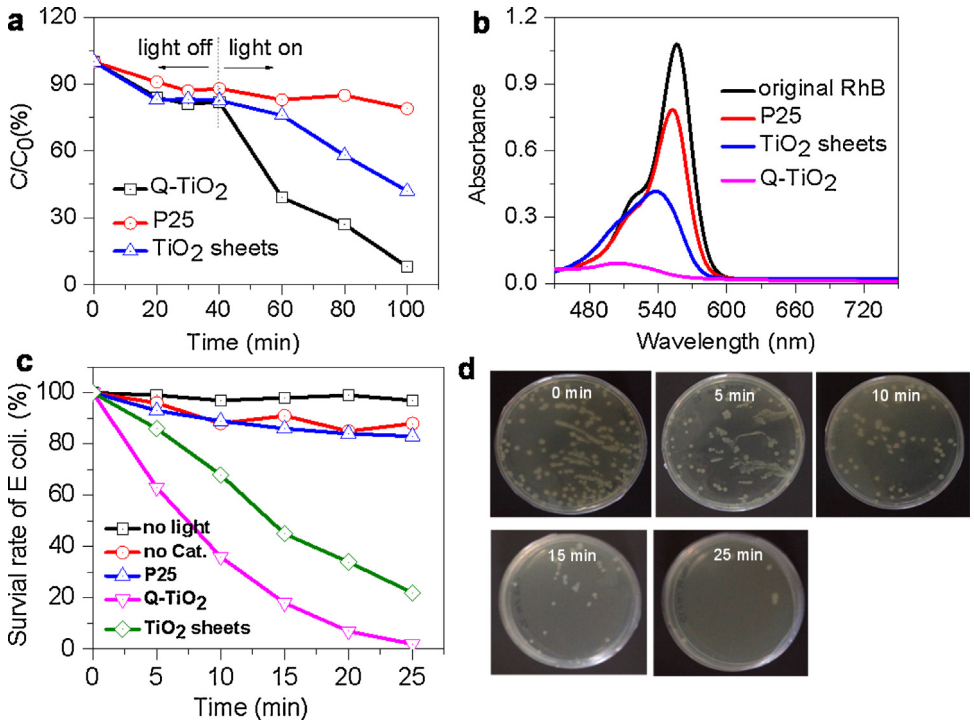

Fig. 7. Photocatalytic properties of Q-TiO_2, TiO_2 sheets, and P25 mateials with visible light ($\lambda \geq 420$ nm): (a) and (b) photocatalytic degradation of organic dye pollutant (Rhodamine B, RhB) and corresponding UV–vis absorption curves; (c) Time-dependent photocatalytic disinfection of bacteria (*E. coli*) from 0 to 25 min. The control includes no light and no catalysts under the same conditions; (d) corresponding pictures of the bacteria E. coli cultured in petri-dishes with light irradiation.

tant (RhB) degradation. This report highlights the key importance of specific surface states of Q-TiO_2 with respected to enhanced photocatalysis. This finding provides a strategy for solar light harvesting in environmental remediation.

Acknowledgements

This work was supported by Ability R&D Energy Research Centre, City University of Hong Kong (SRG-7002919, CityU11207414), National Natural Science Foundation of China (21477079, 21677099), the Ministry of Education of China (PCSIRT_IRT_16R49), and the Shanghai Government (15QA1403300, 13YZ054, 14ZR1430900). We acknowledge the help from Tan Wei Ling about lifetime measurement.

Appendix A. Supplementary data

Supplementary data associated with this article can be found, in the online version, at http://dx.doi.org/10.1016/j.apcatb.2017.05.043.

References

[1] J. Schneider, M. Matsuoka, M. Takeuchi, J. Zhang, Y. Horiuchi, M. Anpo, D.W. Bahnemann, Chem. Rev. 114 (2014) 9919–9986.
[2] K. Fujiwara, Y. Kuwahara, Y. Sumida, H. Yamashita, Langmuir 33 (2016) 288–295.
[3] K.C. Christoforidis, T. Montini, E. Bontempi, S. Zafeiratos, J.J.D. Jaén, P. Fornasiero, Appl. Catal. B: Environ. A. Appl. Catal. B: Environ. 187 (2016) 171–180.
[4] W. Zhang, K.S. Kjær, R. Alonso-Mori, U. Bergmann, M. Chollet, L.A. Fredin, R.G. Hadt, R.W. Hartsock, T. Harlang, T. Kroll, Chem. Sci. 8 (2017) 515–523.
[5] A.J. Nozik, Annu. Rev. Phys. Chem. 52 (2001) 193–231.
[6] S. Kaniyankandy, H.N. Ghosh, J. Mater. Chem. 19 (2009) 3523–3528.
[7] H. Peng, J. Li, S.-S. Li, J.-B. Xia, J. Phys. Chem. C 112 (2008) 13964–13969.
[8] M.R. Gholipour, C.-T. Dinh, F. Béland, T.-O. Do, Nanoscale 7 (2015) 8187–8208.
[9] W.-N. Zhao, S.-C. Zhu, Y.-F. Li, Z.-P. Liu, Chem. Sci. 6 (2015) 3483–3494.
[10] Y.W. Su, W.H. Lin, Y.J. Hsu, K.H. Wei, Small 10 (2014) 4427–4442.
[11] D. Barreca, G. Carraro, A. Gasparotto, C. Maccato, M.E. Warwick, E. Toniato, V. Gombac, C. Sada, S. Turner, G. Van Tendeloo, Adv. Mater. Interfaces 3 (2016).
[12] T. Montini, M. Melchionna, M. Monai, P. Fornasiero, Chem. Rev. 116 (2016) 5987–6041.
[13] A. Fujishima, Nature 238 (1972) 37–38.
[14] C.Y. Teh, T.Y. Wu, J.C. Juan, Catal. Today 256 (2015) 365–374.
[15] H. Cheng, M. Wen, X. Ma, Y. Kuwahara, K. Mori, Y. Dai, B. Huang, H. Yamashita, J. Am. Chem. Soc. 138 (2016) 9316–9324.
[16] K. Hu, A.D. Blair, E.J. Piechota, P.A. Schauer, R.N. Sampaio, F.G. Parlane, G.J. Meyer, C.P. Berlinguette, Nat. Chem. 8 (2016) 853–859.
[17] W. Zhang, L. Wang, H. Liu, Y. Hao, H. Li, M.U. Khan, J. Zeng, Nano Lett. 17 (2017) 788–793.
[18] D. Debellis, G. Gigli, S. ten Brinck, I. Infante, C. Giansante, Nano Lett. 17 (2017) 1248–1254.
[19] J.-C. Blancon, H. Tsai, W. Nie, C.C. Stoumpos, L. Pedesseau, C. Katan, M. Kepenekian, C.M.M. Soe, K. Appavoo, M.Y. Sfeir, S. Tretiak, P.M. Ajayan, M.G. Kanatzidis, J. Even, J.J. Crochet, A.D. Mohite, Science 355 (2017) 1287–1288.
[20] M. Cargnello, T. Montini, S.Y. Smolin, J.B. Priebe, J.J.D. Jaén, V.V. Doan-Nguyen, I.S. McKay, J.A. Schwalbe, M.-M. Pohl, T.R. Gordon, Proc. Natl. Acad. Sci. 113 (2016) 3966–3971.
[21] S. Wang, S.V. Kershaw, G. Li, M.K. Leung, J. Mater. Chem. 3 (2015) 3280–3285.
[22] J. Shi, J. Chen, G. Li, T. An, H. Yamashita, Catal. Today 281 (2017) 621–629.
[23] E.B. Simsek, Appl. Catal. B: Environ. 200 (2017) 309–322.
[24] H. Li, Y. Wang, G. Chen, Y. Sang, H. Jiang, J. He, X. Li, H. Liu, Nanoscale 8 (2016) 6101–6109.
[25] L. Liu, Y. Jiang, H. Zhao, J. Chen, J. Cheng, K. Yang, Y. Li, ACS Catal. 6 (2016) 1097–1108.
[26] Q. Zhu, Y. Peng, L. Lin, C.-M. Fan, G.-Q. Gao, R.-X. Wang, A.-W. Xu, J. Mater. Chem. A 2 (2014) 4429–4437.
[27] X. Chen, L. Liu, P.Y. Yu, S.S. Mao, Science (New York, N.Y.) 331 (2011) 746–750.
[28] C. Mousty-Desbuquoit, J. Riga, J.J. Verbist, J. Chem. Phys. 79 (1983) 26–32.
[29] J. Zhu, W. Zheng, B. He, J. Zhang, M. Anpo, J. Mol. Catal. A: Chem. 216 (2004) 35–43.
[30] E. Wang, W. Yang, Y. Cao, J. Phys. Chem. C 113 (2009) 20912–20917.
[31] L.-B. Xiong, J.-L. Li, B. Yang, Y. Yu, J. Nanomater. 2012 (2012) 9.
[32] M.M. Khan, S.A. Ansari, D. Pradhan, M.O. Ansari, J. Lee, M.H. Cho, J. Mater. Chem. A 2 (2014) 637–644.
[33] K.A. Chan, S.G. Kazarian, Mol. Pharm. 1 (2004) 331–335.
[34] O. Mert, E. Doganci, H. Erbil, A. Demir, Langmuir 24 (2008) 749–757.
[35] S.C. Chang, Y. Ho, M.J. Weaver, J. Am. Chem. Soc. 113 (1991) 9506–9513.
[36] L. de la Garza, Z.V. Saponjic, N.M. Dimitrijevic, M.C. Thurnauer, T. Rajh, J. Phys. Chem. C 110 (2006) 680–686.
[37] H. Park, W. Choi, J. Phys. Chem. B 108 (2004) 4086–4093.
[38] G. Rothenberger, J. Moser, M. Graetzel, N. Serpone, D.K. Sharma, J. Am. Chem. Soc. 107 (1985) 8054–8059.
[39] G.T. Brown, J.R. Darwent, J. Phys. Chem. 88 (1984) 4955–4959.

[40] A.L. Linsebigler, G. Lu, J.T. Yates Jr., Chem. Rev. 95 (1995) 735–758.
[41] V.S. Vyas, V.W. -h. Lau, B.V. Lotsch, Chem. Mater. 28 (2016) 5191–5204.
[42] M. Anpo, M. Che, B. Fubini, E. Garrone, E. Giamello, M.C. Paganini, Top. Catal. 8 (1999) 189–198.
[43] J.M. Coronado, A.J. Maira, J.C. Conesa, K.L. Yeung, V. Augugliaro, J. Soria, Langmuir 17 (2001) 5368–5374.
[44] G. Liu, L.-C. Yin, J. Wang, P. Niu, C. Zhen, Y. Xie, H.-M. Cheng, Energy Environ. Sci. 5 (2012) 9603–9610.
[45] T.K. Das, P. Ilaiyaraja, P.S. Mocherla, G. Bhalerao, C. Sudakar, Sol. Energy Mater. Sol. Cells 144 (2016) 194–209.